American Mineralogist, Volume 69, pages 69–78, 1984

Fugacities of sulfurous gases in pyrrhotite-bearing silicic magmas

JAMES A. WHITNEY

Department of Geology
University of Georgia, Athens, Georgia 30602

Abstract

Thermodynamic data are used to determine the fugacities of sulfurous gases S_2, SO_2 and H_2S along the pyrrhotite saturation surface within the system Fe–S_2–O_2–SiO_2. The fugacities of these species are contoured on diagrams of log fO_2 versus T (°C). These diagrams allow the fugacities of sulfurous species for silicic magmas to be estimated assuming that the temperature and oxygen fugacity are determined from coexisting magnetite and ilmenite, and the pyrrhotite inclusions represent magmatic conditions. In cases where the pyrrhotite was analyzed and the fugacities calculated, the results are consistent. This method is widely applicable because it may be used for any rock for which iron–titanium oxide data are available and igneous pyrrhotite is present.

Both S_2 and SO_2 are highly dependent on fO_2 and T, decreasing with both variables. Sulfur ranges from 10 to 10^{-4} bars whereas SO_2 varies from 10^3 to 10^{-3}. Hydrogen sulfide is less variable, ranging between 100 and 10 bars, but it also decreases with log fO_2 and temperature.

The initial volatile phases evolved at high temperatures from oxidized magmas are rich in SO_2. Volatile separation depletes the magma in sulfur and causes reduction of the magma by oxidation of HS^- in the melt to SO_2 in the vapor phase. Such magmatic volatile phases can be an important source of sulfur for some types of ore deposits.

Introduction

Sulfur dioxide and hydrogen sulfide have long been recognized as important, and odoriferous, components of volcanic emanations. Until recently, the activities of these species have not been quantified in magmas responsible for major silicic volcanism or plutonism, although the high SO_2 activities implied by certain assemblages were noted by several authors (Popp *et al.*, 1977; Tsu *et al.*, 1979). The recognition of pyrrhotite as inclusions in phenocrysts of ash-flow tuffs (Hildreth, 1977; Drexler, 1982; Whitney and Stormer, 1983) allows the activities of these species to be calculated for some occurrences and gives us insight into the importance of sulfur in calc-alkaline silicic magmas prior to near-surface degassing.

When the composition of the pyrrhotite can be carefully determined, the sulfur fugacity can be calculated (Toulmin and Barton, 1964). This value, combined with the fugacity of oxygen and water, and temperature determined from other mineral relationships, allows the fugacities of SO_2, SO_3, and H_2S to be calculated. Unfortunately, the composition of the pyrrhotite is difficult to determine with sufficient accuracy (±0.1 mole% FeS) because of the small size of the inclusions, spontaneous exsolution on quenching, and the effects of oxidation during cooling and devitrification. Therefore, the direct determination of sulfur fugacity can only be done on the freshest, least oxidized samples with large inclusions.

The position of the pyrrhotite–magnetite boundary within the system Fe–O_2–S_2–SiO_2 gives an alternative method of calculating the sulfur fugacity if the temperature and oxygen fugacity are known, as is the case when co-existing iron–titanium oxides are present (Buddington and Lindsley, 1964; Spencer and Lindsley, 1981). This paper develops diagrams from which the fugacity of sulfurous species may be determined assuming primary pyrrhotite inclusions are present, an iron silicate of known thermodynamic character is present, and the temperature and oxygen fugacity are known.

Pyrrhotite occurrence

Pyrrhotite in silicic volcanics is found as round inclusions within phenocryst phases (Hildreth, 1977; Drexler, 1982; Whitney and Stormer, 1983). It has been observed as inclusions within magnetite, mafic silicates, sphene, and plagioclase. It rarely forms euhedral crystals, with the dominant morphology being rounded blebs. To date, it has not been observed or reported within glass. Figure 1 shows typical pyrrhotite inclusions in magnetite. Because the round blebs are found in iron-free plagioclase as well as mafic minerals, the shape is an original morphology

0003–004X/84/0102–0069$02.00

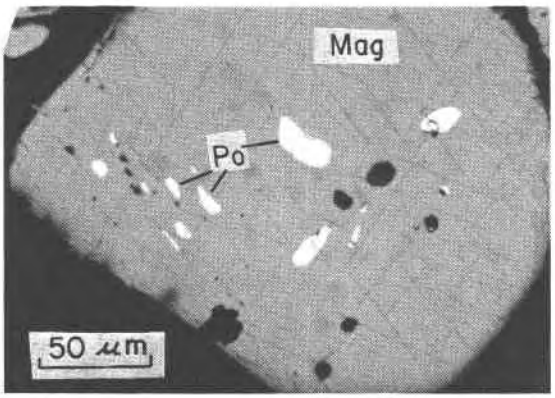

Fig. 1. Typical pyrrhotite inclusions within magnetite from the Fish Canyon Tuff, Central San Juan volcanic field, Southern Colorado (Whitney and Stormer, 1983).

rather than the result of reaction with the host. This shape may be caused by resorption by the melt before inclusion, or it may be an original growth morphology or pseudomorphs after blebs of an immiscible liquid (Whitney and Stormer, 1983).

The best preserved crystals are found in vitric volcanic rocks. During cooling and devitrification the pyrrhotite oxidizes to pyrite and magnetite by reaction with the atmosphere. An idealized end-member reaction is:

$$6\ FeS + 2\ O_2 = 3\ FeS_2 + Fe_3O_4. \qquad (1)$$

Such oxidation can cause an excess of sulfur in the remaining sulfide and destroy the original composition. Sulfur rich pyrrhotites with less than 0.47 iron atoms per formula cannot even be quenched in the laboratory, but spontaneously exsolve to a mixture of lower temperature pyrrhotite and pyrite (Corlett, 1968; Barton, 1969; Craig and Scott, 1974). Therefore, what probably exists in most cases is a fine-grained intergrowth of two phases. Within magnetite, reaction with the host occurs quickly as magnetite begins to re-equilibrate with the exsolution of ulvöspinel or ilmenite accompanying oxidation. Pyrrhotite enclosed within silicate minerals survives longer and can give reliable results in devitrified samples, but great care must be used to assure that the composition analyzed is representative of the original. In many samples, reliable compositions cannot be obtained.

The small size of the inclusions (often less than 10 μm) makes microprobe analysis difficult, especially when they are in iron-bearing phases. Often, only the largest inclusions can be analyzed.

Assuming accurate analyses can be obtained, the sulfur fugacity can be calculated from the composition of the pyrrhotite (Toulmin and Barton, 1964). The results of these calculations are sensitive to the ratio of iron to sulfur, and thus the analytical uncertainty in microprobe analyses (approximately ±2%) causes more than an order of magnitude error in sulfur fugacity. This uncertainty leads to larger errors in SO_2, and significant uncertainty in H_2S.

Due to all these problems, it is desirable to develop an alternative method for use when the original pyrrhotite composition is altered or accurate analyses are not possible. The position of the magnetite–pyrrhotite boundary within the system Fe–O_2–S_2–SiO_2 provides such a method. In volcanic rocks, the temperature and oxygen fugacity are often known as well as any intensive magmatic variables due to the occurrence of coexisting magnetite and ilmenite solid solutions (Buddington and Lindsley, 1969; Spencer and Lindsley, 1981). These variables, combined with the position of the pyrrhotite–magnetite boundary in the simple system, can be used to estimate the fugacity of various sulfurous species without relying on the pyrrhotite analyses. Such a method also allows a check on the results of pyrrhotite analyses.

Phase diagrams for the system Fe–O_2–S_2–SiO_2

The most useful diagram for the present purpose is that in which the fugacities of O_2 and S_2 are used as coordinates. The details of constructing such diagrams have been discussed by many authors (*e.g.*, Garrels and Christ, 1965; Holland, 1959, 1965). Sources of thermodynamic data are summarized in Table 1. Isothermal diagrams for various temperatures are shown in Figure 2.

The calculation of the pyrrhotite–magnetite curve is of special importance for current application. Because pyrrhotite varies in composition with changing sulfur fugacity (Toulmin and Barton, 1964), this boundary is slightly concave to the lower left. It originates at a triple point (magnetite–triolite–iron), which is metastable above 570°C due to the stability of wüstite and metastable at all temperatures in the presence of quartz. For our purposes, however, this triple point may be used as the origin of the curve throughout the temperature range examined because the thermodynamic properties of all three phases are well known. The pyrrhotite–magnetite boundary may be constructed graphically by determining the slope of the line for the composition of pyrrhotite stable at a certain

Table 1. Sources of thermodynamic data

Equilibria	Source of data
$2\ Fe + S_2 = 2\ FeS$	Barton and Skinner, 1979
$3/2\ Fe + O_2 = 1/2\ Fe_3O_4$	Barton and Skinner, 1979
$4\ Fe_3O_4 + O_2 = 6\ Fe_2O_3$	Barton and Skinner, 1979
$S_2 = 2\ S(L)$	Barton and Skinner, 1979
$3\ Fe_3O_4 + S_2 = FeS_2 + 4\ Fe_2O_3$	Barton and Skinner, 1979
$2/5\ Fe_3O_4 + S_2 = FeS_2 + 2/5\ FeSO_4$	Barton and Skinner, 1979
$Fe_{1-x}S + \frac{1-2x}{2} S_2 = (1-x)\ FeS_2$	Toulmin and Barton, 1964
$1/2\ S_2 + O_2 = SO_2$	Robie et al., 1979
$1/2\ S_2 + H_2 = H_2S$	Robie et al., 1979
$H_2 + 1/2\ O_2 = H_2O$	Robie et al., 1979
$2\ Fe_3O_4 + 3\ SiO_2 = 3\ Fe_2SiO_4 + O_2$	Robie et al., 1979
$1/2\ S_2 + 3/2\ O_2 = SO_3$	Robie et al., 1979

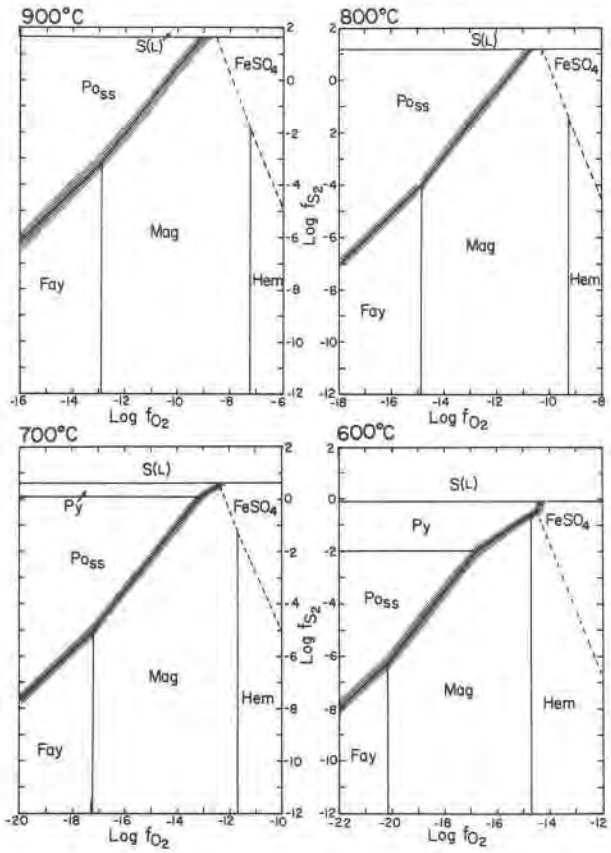

Fig. 2. Isothermal, quartz saturated, log fO_2 *vs.* log fS_2 diagrams for the system Fe–O_2–S_2–SiO_2. Calculated as described in the text and Appendix from sources listed in Table 1. The sulfide saturation surface is shown in gray. S(L) = sulfur liquid, Po_{ss} = pyrrhotite solid solution, Fay = fayalite, Mag = magnetite, Hem = hematite, Py = pyrite.

sulfur fugacity, drawing a short section of the curve as a straight line, changing the composition of the pyrrhotite, and repeating the process. Alternatively, the curve may be calculated using equation (8) of Toulmin and Barton (1964) and the coordinates of the triple point (see Appendix). Both methods were used and gave satisfactory results.

These diagrams may be further contoured for fugacity of SO_2 and H_2S (Fig. 3). To determine H_2S some measure of hydrogen fugacity must be made. It is convenient to estimate the fugacity of H_2O and use its dissociation constant to give fH_2 as a function of fO_2 and T. As a consequence, the H_2S isopleths vary with water fugacity. The intersections of the contour lines with the sulfide boundary on these diagrams may be transferred to an fO_2 and T diagram to represent the values along the sulfide saturation surface.

Figure 4 summarizes the various reactions encountered in the Fe–O_2–S_2–SiO_2 system projected onto a log fO_2–T diagram. Also shown are the approximate fO_2–T conditions for various pyrrhotite-bearing volcanic rocks. Most of these magmas are moderately oxidizing, with the exception of the Bishop Tuff. All fall within the calculated stability field of pyrrhotite, which is consistent with the observed paragenesis. Several occurrences show a more reducing trend at lower temperatures than would be expected from simple movement along magmatic buffer curves that are controlled by fixed ferric/ferrous ratios in the melt (Sack *et al.*, 1980). Carbon species oxidation–reduction lie at far more reducing conditions than these rocks indicate, and thus methane, graphite, or carbon monoxide play trivial roles in these silicate melts.

Figure 5 shows the fugacity of sulfur contoured on the same log fO_2–T diagram. The fS_2 isopleths are flatter than the simple buffer curves of Figure 4, and are probably flatter than the more complex buffers that control silicate magma crystallization. Therefore, lowering temperatures lead to lowering sulfur fugacities. The approximate range

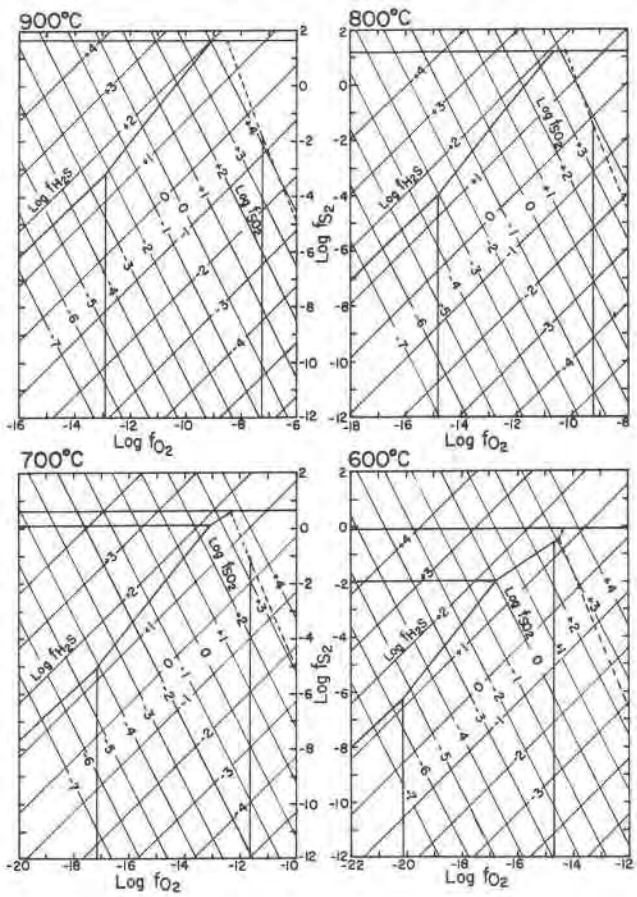

Fig. 3. Isothermal log fO_2 versus log fS_2 diagrams contoured for log fSO_2 and log fH_2S. Stability fields are the same as in Fig. 2, with contours calculated using data from Robie *et al.* (1979). Fugacity of H_2O is 2000 bars.

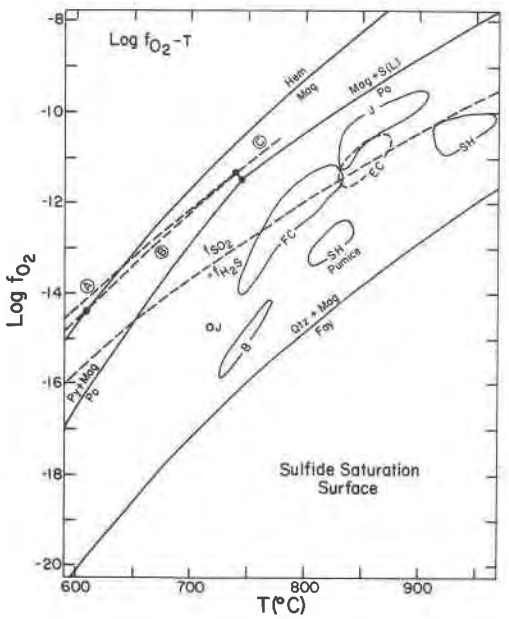

Fig. 4. Log fo_2–T diagram for the sulfide-saturated equilibria. Reactions involving $FeSO_4$ are only approximately known and are labeled as follows: A. $FeSO_4$+ S(L) = pyrite; B. $FeSO_4$ = magnetite + pyrite; C. $FeSO_4$ = magnetite + S(L). Conditions for various pyrrhotite-bearing volcanic rocks are shown. B = Bishop Tuff, Hildreth (1977, 1979); FC = Fish Canyon Tuff, Whitney and Stormer (1983); J = Julcani vitrophyres, Drexler (1982); SH = St. Helens ash, Melson and Hopson (1981). All of the above were recalculated from coexisting iron–titanium oxides using the equations of Spencer and Lindsley (1981) and Stormer (1983). Also shown is the approximate conditions of the El Chichón ash. Although ilmenite is absent, the presence of sphene in place of ilmenite restricts the possible oxygen fugacity. Phenocryst assemblage and approximate conditions taken from Luhr *et al.* (1982).

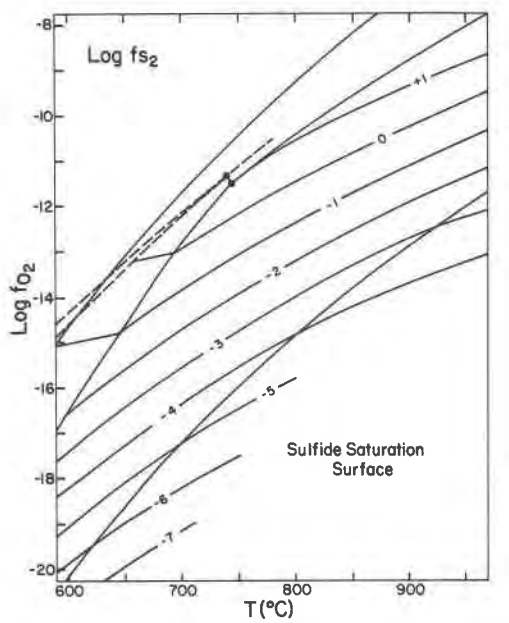

Fig. 5. Log fo_2 *vs.* T diagram portraying contours of constant log fs_2 on the sulfide saturation surface. Reaction lines are the same as in Fig. 4.

of values is 10 to 10^{-2} bars at 950°C down to 10^{-1} to 10^{-4} bars at 700°C.

Figure 6 shows a similar projection of SO_2 contours. In this case, the curves are even more closely spaced so that a small decrease in oxygen fugacity makes a drastic decrease in fSO_2. A change of 0.5 log fo_2 changes log fSO_2 by 1.0 at constant log fs_2. The fugacity of SO_2 tends to decrease with decreasing temperature along standard magmatic buffer curves, with an average range of values decreasing from 10^3 to 10^{-1} at 950°C to 10 to 10^{-3} at 700°C.

The fugacity of H_2S (Fig. 7) is much less variable, always between 10 and 100 bars, and is dependent on water fugacity. The diagram shown here is for 2000 bars fH_2O. Values may be corrected to other water fugacities by adding the term log (fH_2O/2000) to the raw values. The fH_2S again tends to decrease with decreasing temperature along magmatic buffer curves, but the change is much smaller in magnitude.

Perturbations caused by pressure and solid solution

Pressure correction

The pyrrhotite–magnetite curve is shifted slightly by changes in confining pressure. This effect is a result of two factors: the change in the origin of the curve con-

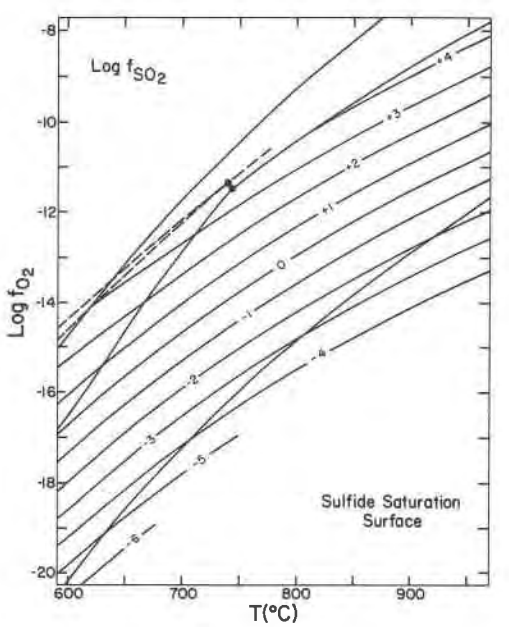

Fig. 6. Log fo_2 *vs.* T diagram portraying contours of constant log fSO_2 on the sulfide saturation surface. Reaction lines are the same as in Fig. 4.

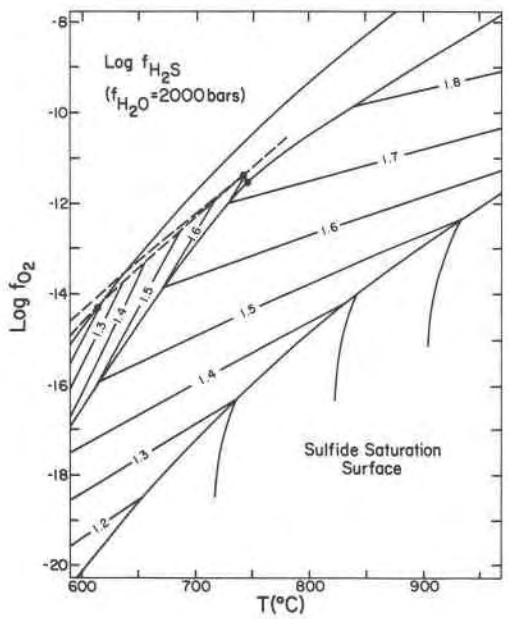

Fig. 7. Log fo_2 *vs.* T diagram portraying contours of constant log f_{H_2S} on the sulfide saturation surface for a water fugacity of 2000 bars. To convert to other water fugacities add the term log f_{H_2S}/200. Reaction lines are the same as in Fig. 4.

trolled by the magnetite–iron and troilite–iron equilibria, and the change in pyrrhotite composition for a specific sulfur fugacity resulting in a change in the slope of the curve. The first effect is by far the most significant, and is the only one causing significant perturbations at crustal pressures (see Appendix for detailed derivation of the curve).

The equilibria controlling the starting point of the curve can be corrected for confining pressure by adding a $P\Delta V$ term to the Gibbs free energy of the reaction. These terms for both equilibria are listed in Table A-2 (Appendix) as a function of temperature. The shift in the boundary itself in terms of the change in log fs_2 per kilobar at constant log fo_2 is tabulated in the fourth column of Table A-2 (see appendix for derivation and tabulation). This value will be represented in subsequent equations as the parameter (A).

To correct the values of log fs_2 obtained from Figure 5 for pressure, a term must be added that has approximately the magnitude $A \cdot P$ where P is confining pressure in kilobars. Both log fso_2 and log f_{H_2S} must be corrected by adding a term $A/2 \cdot P$ (see Appendix for derivation).

Solid solution in magnetite and pyrrhotite

Solid solution in magnetite, dominantly in the form of ulvöspinel, shifts the magnetite–pyrrhotite boundary to higher sulfur fugacities by decreasing the activity of magnetite. Similarly, solid solution of other cations for iron in pyrrhotite shifts the boundary to slightly lower sulfur fugacities (less than 0.05 log fs_2 for natural pyrrhotites). These changes can also be modelled by considering the effects of such solid solutions on the magnetite–iron and troilite–iron starting point for the curve (see Appendix). If these shifts in the curve are given as changes in log fs_2 for a fixed log fo_2, they take on the following values (see Appendix for derivation).

$$\Delta(\log fs_2)_{\text{Solid Solution}} = 2 \log a_{po} - \frac{2}{3} \log a_{mag} \quad (2)$$

To a good first approximation, the a_{mag} may be replaced by the mole fraction of magnetite in the magnetite solid solution calculated by an appropriate method (see for example Stormer, 1983). The deficiency of iron in the pyrrhotite is already accounted for in the algebraic expression for the curve (see Appendix). Therefore, the only parameter affecting the activity of pyrrhotite is the substitution for iron. In addition, the a_{po} may be replaced by the number of moles of iron divided by the total number of cations. The resulting correction takes the form:

$$\Delta(\log fs_2)_{\text{Solid Solution}} = 2 \log X_{Fe}^{po} - \frac{2}{3} \log X_{Fe_3O_4}^{mag} \quad (3)$$

where

$$X_{Fe}^{po} = \frac{N_{Fe}}{N \text{ Cations}} \quad (4)$$

The corrections for both log fso_2 and log f_{H_2S} are 1/2 the value for log fs_2 (see Appendix for detailed derivation).

Procedure for calculating fugacities

In order to obtain the most accurate estimates of fugacity for S_2, SO_2, and H_2S from the figures described in the previous section, the following procedure should be followed:

1. Carefully examine polished sections to insure that pyrrhotite appears to be a primary phase in equilibrium with the phenocryst assemblage.
2. Determine the composition of coexisting magnetite and ilmenite solid solutions using standard microprobe techniques or other analytical methods.
3. Calculate the temperature and oxygen fugacity of equilibrium using the most recent solution model for magnetite–ilmenite solid solutions and an appropriate method for calculating mole fractions (currently Spencer and Lindsley, 1981 and Stormer, 1983 are recommended).
4. Plot the coordinates derived on Figures 5, 6, and 7 to obtain raw values of log fs_2, log fso_2, and log f_{H_2S}. These values will be referred to as (log fs_2)′, (log fso_2)′, and (log f_{H_2S})′.
5. If possible, estimate the probable water fugacity and total confining pressure on the magma during phenocryst equilibration. In many cases only crude approximations

are available, but because the perturbations are small the results are still satisfactory.

6. If possible, determine the approximate composition of the pyrrhotite to check for the presence of significant copper or nickel substituting for iron.

7. Correct the raw values according to the following equation:

$$\log fS_2 = (\log fS_2)' + A \cdot P(\text{kbar}) - \frac{2}{3}\log X^{mag}_{Fe_3O_4} + 2 \log X^{po}_{Fe} \quad (5)$$

$$\log fSO_2 = (\log fSO_2)' + \frac{A}{2} \cdot P(\text{kbar}) - \frac{1}{3}\log X^{mag}_{Fe_3O_4} + \log X^{po}_{Fe} \quad (6)$$

$$\log fH_2S = (\log fH_2S)' + \log \frac{fH_2O}{2000} + \frac{A}{2} \cdot P(\text{kbar}) - \frac{1}{3}\log X^{mag}_{Fe_3O_4} + \log X^{po}_{Fe}. \quad (7)$$

The values of A for these equations should be selected for the appropriate temperature from Table A-2. Other parameters are as defined in previous sections.

Calculations for specific occurrences

Table 2 summarizes the results for a number of silicic rocks for which pyrrhotite was reported as a primary phase. Values in parenthesis were calculated from the pyrrhotite analyses and are approximate values due to the uncertainties previously described. In each case, these values vary by an order of magnitude depending on the actual analysis used. The correlation between the two methods is therefore good within the uncertainty inherent in both methods. The corrections for pressure, solid solution, and water fugacity are small, generally less than 0.2 log units. Therefore, even in cases where these variables are poorly known, the raw values for fugacities are still useful estimates.

The uncertainties in both methods are significant and should be considered in comparing data from different sources. When calculating the sulfur fugacity directly from the pyrrhotite composition, it must be assumed that the analysis represents the original bulk composition and no exsolution or oxidation has changed the bulk composition significantly. Such occurrences are rare, but assuming this is the case the normal uncertainty in microprobe analyses is still ±2% of the amount present. This error in pyrrhotite composition translates into approximately a ±1.5 uncertainty in log fS_2 at moderately high oxygen fugacity. The calculation of log fSO_2 and log fH_2S are less certain because the values of fO_2 and fH_2O must be estimated from other mineralogical relationships.

Using the method described in this paper there are two important sources of error. The most important is the uncertainty in oxygen fugacity and temperature inherent in the magnetite–ilmenite geothermometer. According to Spencer and Lindsley (1981) this error is 40 to 80° and 0.5 to 1.0 log fO_2. These, however, are not independent as analytic errors cause movement of both variables. Their estimated uncertainty, when plotted on Figure 5, yields an uncertainty of less than ±1.0 in log fS_2. A second source of error is in the position of the pyrrhotite–magnetite curve. During the course of this study, various thermodynamic parameters were used to calculate the curve. In no case was the discrepancy more than ±0.2 in log fS_2. The combined uncertainty using the magnetite–pyrrhotite boundary therefore appears to be equal to, or less than, the analytic uncertainty inherent in the analysis of pyrrhotite. More importantly, the current method is applicable to cases where the pyrrhotite has exsolved or oxidized, and may be applied in any case where primary pyrrhotite is present and fO_2 and temperature can be estimated.

Using the diagrams of this study, maximum limits can even be placed on the fugacity of these sulfurous gases in

Table 2. Fugacity of sulfurous species in parent magmas for some pyrrhotite-bearing silicic volcanic rocks.

	T(°C)	Log fO_2	Log fS_2		Log fSO_2		Log fH_2S		fS_2	fSO_2	fH_2S
			Uncorr.	Corr.	Uncorr.	Corr.	Uncorr.	Corr.			
Bishop	770	-14.4	-2.9	-2.7	-1.6	-1.5	+1.47	+1.62	0.002 (0.005)	0.03 (0.10)	36 (40)
Fish Canyon	800	-11.6	-0.2	+0.2	+2.1	+2.2	+1.69	+1.88	1.6 (2.0)	160 (150)	76 (80)
Julcani	880	- 9.8	+0.8	+0.9	+3.2	+3.2	+1.78	+1.73	8 (5)	1600 (350)	54 (35)
St. Helens	950	-10.2	-0.6	-0.4	+1.2	+1.3	+1.71	+1.52	0.4	20	33
El Chichón	850	-11.0	-0.2	0.0	+2.0	+2.1	+1.71	+1.67	1.0	125	47

Note: All fugacities are in bars. Numbers in parentheses are average values calculated from chemical analyses of pyrrhotite. All other estimates determined as described in this paper. Data recalculated from the following sources: Bishop, Hildreth (1977); Fish Canyon, Whitney and Stormer (1983); Julcani, Drexler (1982); St. Helens, Melson and Hopson (1981); El Chichón, Luhr et al. (1982). All temperatures and log fO_2 values recalculated from the original data using the expression of Spencer and Lindsley (1981) and Stormer (1982). Fugacity of water estimated in different ways by various authors. El Chichón data is only approximate due to the lack of ilmenite in the phenocryst assemblage.

volcanic rocks that do not have primary pyrrhotite. The absence means their fugacity falls below the boundary. It therefore appears that the current method is at least as accurate as calculations based on microprobe analyses of pyrrhotite, and is much more widely applicable.

Role of sulfurous gases in silicic magmas

Examination of Figures 5, 6, and 7 demonstrates that SO_2 and H_2S are the dominant sulfurous species in gases equilibrated with pyrrhotite-bearing magmas. Calculations of SO_3 fugacity show it to be from 2 to 10 orders of magnitude less than SO_2, so that it is never a dominant species. The values obtained for SO_2 may be quite high for oxidizing magmas, and in some cases it may be a dominant component of the gaseous phase. Hydrogen sulfide is far less variable, generally being in the tens of bars. It is significant for all conditions of fo_2 and T.

Under closed system conditions, the fugacities of all sulfur species decrease with decreasing temperature along normal magmatic buffer curves through the precipitation of pyrrhotite. This pattern permits pyrrhotite to remain stable; however, separation of the volatile phase severely alters this process.

As a silicic magma rises toward the surface, early volatile phases will have approximately the fugacities calculated for the parent magma. The magma, however, probably has a rather low abundance of sulfur dissolved in the melt (Burnham, 1979). Therefore as early volatile phases separate, the melt is rapidly depleted in sulfur. Under oxidizing conditions, the amount of SO_2 in early volatile emanations may be rather large, but very little of this component can be derived from a sulfur-poor melt. Any sulfide in contact with the melt would probably react to release sulfur. This process may explain why pyrrhotite is not reported in the glass of silicic volcanic rocks, but is only included in other phases. Certainly, the majority of the sulfur dissolved in the melt would be released during degassing accompanying eruption, so that whole-rock sulfur values of tuffs are much lower than the values in the parent magma.

Although there is no direct evidence as to the sulfur species present in the melt, Burnham (1979) has hypothesized that the dominant one is HS^- based on H_2O and CO_2 as analogs for H_2S and SO_2 respectively. This assumption awaits experimental confirmation, but if it is true, separation of an SO_2-rich gas phase would take oxygen from the melt to form SO_2, causing a reduction in fo_2 even at constant temperature. This phenomenon may explain why analyses from Julcani and the Fish Canyon Tuff (Fig. 4) show a trend to lower oxygen fugacities at low temperatures greater than would be expected for common magmatic buffer curves.

Early-formed magmatic volatiles rich in SO_2 may be important sources of sulfur for metallic ore deposits. These volatile phases would also preferentially concentrate chlorine from the magma, which would help transport metallic elements in solution. Oxidizing magmatic conditions evidenced by the early formation of sphene would be beneficial to the formation of such solutions.

One important question is the source of sulfur for these silicic magmas. In the exceptional case of El Chichón, the high SO_2 content may have been derived by assimilation of sulphates from evaporites in the upper crust (Luhr *et al.*, 1982). In other cases, sulfides deposited in volcanic crust by hydrothermal circulation at ocean ridges may be an important source of sulfur. If the examples studied so far are typical, then many calc-alklaine magmas were saturated with pyrrhotite at an early stage and must have had a sulfide-rich protolith. Altered oceanic crust also helps explain the oxidized conditions of these magmas, as oxidation accompanies both the reduction of sulphate in sea water in hydrothermal systems, and the conversion of pyrite to pyrrhotite during metamorphism (Whitney and Stormer, 1983).

Conclusions

The fugacity of sulfurous gases in pyrrhotite-bearing magmas can be estimated from temperature and oxygen fugacity with an accuracy equal to, or better-than, calculations based on analyses of the pyrrhotite composition. In addition, the method outlined herein is not affected by the small size of the pyrrhotite or exsolution and oxidation accompanying eruption and deposition.

The sulfur fugacity in pyrrhotite-bearing magmas is between 10 and 10^{-4} bars and decreases with temperature and oxygen fugacity. The fugacity of sulfur dioxide is between 10^3 and 10^{-3} bars, also decreasing with temperature and oxygen fugacity. Hydrogen sulfide fugacity is less variable, between 10 and 100 bars, but is dependent on water fugacity.

The initial volatile phase evolved at high temperatures from oxidized magmas is rich in SO_2. Separation of the volatile phase rapidly depletes the melt of sulfur, greatly lowering the whole-rock sulfur content and may reduce the oxygen fugacity in the melt below that expected for buffer curves controlled by constant ferric–ferrous iron ratios.

All volcanic materials should be carefully studied to identify the occurrence of pyrrhotite as it appears to be rather common in a number of calc-alkaline silicic rocks. Its occurrence has important consequences for the origin and evolution of such magmas.

Acknowledgments

This research was supported by NSF grant no. EAR-8204568 and with the support and cooperation of the U.S. Geological Survey. Part of the mathematical derivation was inspired by T. Stanley. Helpful ideas and contributions were made by J. C. Stormer, Jr., W. Rose, and J. W. Drexler. The manuscript was greatly improved by reviews from P. Barton, J. Craig, and M. Cameron.

References

Barton, P. B., Jr. (1969) Thermochemical study of the system Fe–As–S. Geochemica et Cosmochimica Acta, 33, 841–857.

Barton, P. B., Jr. (1970) Sulfide petrology. Mineralogical Society of America Special Paper Number 3, 187–198.

Barton, P. B., Jr. and Skinner, B. J. (1979) Sulfide mineral stabilities. In Barnes, H. L., Ed., Geochemistry of Hydrothermal Ore Deposits, 2nd Editions. p. 278–403, Wiley, New York.

Buddington, A. F. and Lindsley, D. H. (1964) Iron titanium oxide minerals and synthetic equivalents. Journal of Petrology, 5, 310–357.

Burnham, C. W. (1979) Magmas and hydrothermal fluids. In Barnes, H. L., Ed., Geochemistry of Hydrothermal Ore Deposits, 2nd Edition, p. 71–136, Wiley, New York.

Corlett, M. (1968) Low-iron polymorphs in the pyrrhotite group. Zeitschrift für Kristallographie, 126, 124–134.

Craig, J. R. and Scott, S. D. (1974) Sulfide phase equilibria. In Mineralogical Society of America Short Course Notes, Volume 1, Sulfide Mineralogy, p. CS-1 to CS-110. Washington D.C.

Drexler, J. W. (1982) Magmatic conditions from vitric units of the Julcani district, Peru. PhD. dissertation (unpublished), Michigan Technological University, Houghton, Michigan.

Garrels, R. M. and Christ, C. L. (1965) Solutions, Minerals, and Equilibria. Harper and Row, New York.

Hildreth, E. W. (1977) The magma chamber of the Bishop Tuff: Gradients in temperature, pressure, and composition. PhD. dissertation (unpublished) University of California, Berkeley.

Hildreth, E. W. (1979) The Bishop Tuff. Evidence for the origin of compositional zonation in silicic magma chambers. In Chapin, C. E., and Elston, W., Eds., Ash Flow Tuffs, p. 43–75, Geological Society of America Special Paper 180.

Holland, H. D. (1959) Some applications of thermochemical data to problems of ore deposits. I. Stability relations among the oxides, sulfides, sulfates and carbonate of ore and gangue minerals. Economic Geology, 54, 184–233.

Holland, H. D. (1965) Some applications of thermochemical data to problems of ore deposits. II. Mineral assemblages and the composition of ore-forming fluids. Economic Geology, 60, 1101–1166.

Luhr, J., Carmichael, I. S. E., and Varekamp, J. C. (1982) eruption of El Chichón volcano, Chiapas Mexico (abstract) EOS (Transactions of the American Geophysical Union), 63, 1126–1127.

Melson, W. G. and Hopson, C. A. (1981) Pre-eruption temperatures and oxygen fugacities in the 1980 eruption sequence. In Lipman, P. W. and Mullinax, D. R., Eds., The 1980 Eruption of Mount St. Helens, Washington, U. S. Geological Survey Professional Paper 1250, p. 641–648.

Popp, R. K., Gilbert, N. C., and Craig, J. R. (1977) Stability of Fe–Mg amphiboles with respect to sulfur fugacity. American Mineralogist, 62, 13–30.

Robie, R. A., Hemingway, B. S., and Fisher, J. O. (1979) Thermodynamic properties of minerals and related substances at 298.15 K (25°C) and one bar (10^5 pascals) pressure and at higher temperatures (revised 1979). U.S. Geological Survey Bulletin 1452. (originally printed in 1978).

Sack, R. O., Carmichael, I. S. E., Rivers, M, and Ghiarso, M. S. (1980) Ferric–ferrous equilibria in natural silicate liquids at 1 bar. Contributions to Mineralogy and Petrology, 75, 369–376.

Spencer, K. J. and Lindsley, D. H. (1981) A solution model for coexisting iron-titanium oxides. American Mineralogist, 66, 1189–1201.

Stormer, J. C., Jr. (1983) The effects of recalculation on estimates of temperature and oxygen fugacity from analyses of multicomponent iron–titanium oxides. American Mineralogist, 68, 586–594.

Toulmin, P., III and Barton, P. B., Jr. (1964) A thermodynamic study of pyrite and pyrrhotite. Geochimica et Cosmochimica Acta, 28, 641–671.

Tsu, J. L., Gilbert, M. C., and Craig, J. R. (1979) Sulfidation of synthetic biotite. American Mineralogist, 64, 304–316.

Whitney, J. A. and Stormer, J. C. Jr., (1983) Igneous sulfides in the Fish Canyon Tuff and the role of sulfur in calc-alkaline magmas. Geology, 11, 99–102.

Manuscript received, December 13, 1982; accepted for publication, July 19, 1983.

Appendix: Thermodynamic Determination of the Pyrrhotite-Magnetite Boundary

The position of the magnetite-pyrrhotite boundary within the system Fe-S_2-O_2 may be determined algebraically assuming that one point on the curve is known, and that the composition of the pyrrhotite is known relative to the sulfur fugacity.

The reaction of the curve may be written in the form

$$(8)\quad 3\,Fe_xS + 2x\,O_2 = x\,Fe_3O_4 + 3/2\,S_2$$

where x is the mole fraction of FeS in a formula unit of pyrrhotite within the system Fe-S. The slope of the magnetite-pyrrhotite boundary on the log f_{S_2}-log f_{O_2} diagram can be derived from the equilibrium constant equation:

$$(9)\quad \log K = 3/2 \log f_{S_2} + x \log a_{mag} - 2x \log f_{O_2} - 3 \log a_{po}\ ,$$

$$(10)\quad 2x \log f_{O_2} = -\log K + 3/2 \log f_{S_2}\ ,$$

assuming that the activity of magnetite and pyrrhotite are unity in the formulas as written. Differentiating yields the slope of the curve:

$$(11a)\quad \frac{d(\log f_{O_2})}{d(\log f_{S_2})} = \frac{3}{4x}\ ,\quad \text{or}\quad (11b)\quad d(\log f_{O_2}) = \frac{3}{4x}\, d(\log f_{S_2})\ .$$

Integrating (11b) from some starting point (o) to some end point (n) will determine the change in log f_{O_2} along the curve:

$$(12)\quad \int_{(\log f_{O_2})_o}^{(\log f_{O_2})_n} d(\log f_{O_2}) = \int_{(\log f_{S_2})_o}^{(\log f_{S_2})_n} \frac{3}{4x}\, d(\log f_{S_2})$$

$$(13)\quad (\log f_{O_2})_n - (\log f_{O_2})_o = \int_{(\log f_{S_2})_o}^{(\log f_{S_2})_n} \frac{3}{4x}\, d(\log f_{S_2})\ .$$

Since the log f_{S_2} is known as a function of mole fraction of pyrrhotite (N in equation 8 of Toulmin and Barton, 1964), the chain rule may be used to change the variable of integration:

$$(14)\quad d(\log f_{S_2}) = \frac{d(\log f_{S_2})}{dN}\, dN$$

$$(15)\quad (\log f_{O_2})_n - (\log f_{O_2})_o = \int_{N_o}^{N_n} \frac{3}{4x} \frac{d(\log f_{S_2})}{dN}\, dN \quad .$$

The log f_{S_2} is given by Toulmin and Barton (1964, equation 8) as:

$$(16)\quad \log f_{S_2} = (70.03 - 85.83\,N)\left(\frac{1000}{T} - 1\right) + 39.3\sqrt{1-0.9981\,N} - 11.91,$$

where T is in °K and N is the mole fraction of FeS in pyrrhotite within the system FeS-S_2. However, since Toulmin and Barton defined N within the system FeS-S_2, rather than FeS-S as done in equation (8), the x in equation (15) must also be replaced by its equivalent in terms of N. This equality takes the form

$$(17a)\quad N = \frac{x}{x+(1-x/2)}\ , \quad (17b)\quad x = \frac{N}{2-N}\ .$$

Differentiating equation (16) and substituting the results along with (17b) into (15), we get the following:

$$(18)\quad \frac{d(\log f_{S_2})}{dN} = -85.85\left(\frac{1000}{T} - 1\right) - \frac{19.613}{\sqrt{1-0.9981\,N}}\ ;$$

$$(19)\quad (\log f_{O_2})_n - (\log f_{O_2})_o = \int_{N_o}^{N_n} \frac{3}{4}\left(\frac{2-N}{N}\right)\left[-85.83\left(\frac{1000}{T} - 1\right) - \frac{19.613}{\sqrt{1-0.9981\,N}}\right] dN$$

$$(20)\quad = -64.37\left(\frac{1000}{T} - 1\right)\left[\int_{N_o}^{N_n} \frac{2}{N}\, dN - \int_{N_o}^{N_n} dN\right] - 14.71\left[\int_{N_o}^{N_n} \frac{2}{N\sqrt{1-0.9981\,N}}\, dN - \int_{N_o}^{N_n} \frac{1}{\sqrt{1-0.9981\,N}}\, dN\right]$$

$$(21)\quad = -64.37\left(\frac{1000}{T} - 1\right)\left[2\ln N - N\right]_{N_o}^{N_n} - 14.71\left[-4\,\mathrm{Tanh}^{-1}\sqrt{1-0.9981\,N} - \left(\frac{2\sqrt{1-0.9981\,N}}{-0.9981}\right)\right]_{N_o}^{N_n} .$$

If we use the magnetite-troilite-iron triple point as a starting point for integration, since this point is well determined thermodynamically and the composition of the pyrrhotite is stoichiometric, then N_o is 1.0 and we get the following result:

$$(22)\quad (\log f_{O_2})_n - (\log f_{O_2})_o = -64.37\left(\frac{1000}{T} - 1\right)(2\ln N - N + 1) + 29.42\left[2\,\mathrm{Tanh}^{-1}\sqrt{1-0.9981\,N} - \frac{\sqrt{1-0.9981\,N}}{0.9981} - 0.0435\right], \text{ or}$$

$$(23)\quad (\log f_{O_2})_n = -64.37\left(\frac{1000}{T} - 1\right)(2\ln N - N + 1) + 29.42\left[2\,\mathrm{Tanh}^{-1}\sqrt{1-0.9981\,N} - \frac{\sqrt{1-0.0091\,N}}{0.9981} - 0.0435\right] + (\log f_{O_2})_o \quad .$$

The oxygen fugacity of the starting point is controlled by the reaction

$$(24)\quad 3/2\ Fe + O_2 = 1/2\ Fe_3O_4$$

with the oxygen fugacity given by

$$(25)\quad \log f_{O_2} = \frac{\Delta G}{2.303\,RT}\ ;\ \Delta G = -131{,}699 + 36.93\,T(^\circ K)$$

for ΔG in calories (Barton and Skinner, 1979). Substituting ΔG into (25) we get

$$(26)\quad (\log f_{O_2})_o = \frac{-28{,}777}{T} + 8.069\ .$$

Substituting this result into (23), we get

$$(27)\quad \log f_{O_2} = -64.37\left(\frac{1000}{T} - 1\right)(2\ln N - N + 1) + 29.42\left(2\,\mathrm{Tanh}^{-1}\sqrt{1-0.9981\,N} - \frac{\sqrt{1-0.9981\,N}}{0.9981}\right) + 6.789 - \frac{28{,}777}{T}\ .$$

Combining the 1/T terms to simplify the expression, we obtain the following equation for oxygen fugacity as a function of N along the curve:

$$(28)\quad \log f_{O_2} = \left[-28.777 - 64.37(2\ln N - N + 1)\right]\left(\frac{1000}{T} - 1\right) + 29.42\left(2\,\mathrm{Tanh}^{-1}\sqrt{1-0.9981\,N} - \frac{\sqrt{1-0.9981\,N}}{0.9981}\right) - 21.99\ .$$

Equations (16) and (28) then specify both sulfur and oxygen fugacity as functions of N. Substituting values of N allows points along the curve to be calculated. By choosing sufficient numbers of N values, the curve may be determined to any required precision. Table A-1 lists examples of values calculated using equations (16) and (28).

Table A-1. Fugacity of oxygen and sulfur along the pyrrhotite–magnetite boundary.

	N_{FeS} in Pyrrhotite										
	1.00	0.99	0.98	0.97	0.96	0.95	0.94	0.93	0.92	0.91	0.90
600°C											
Log f_{O_2}	-24.89	-22.85	-21.58	-20.53	-19.61	-18.75	-17.97	-17.21	-16.48	-15.78	-15.09
Log f_{S_2}	-13.11	- 9.80	- 8.14	- 6.82	- 5.67	- 4.64	- 3.69	- 2.80	- 1.97	- 1.18	- 0.42
700°C											
Log f_{O_2}	-21.50	-19.54	-18.34	-17.37	-16.53	-15.77	-15.06	-14.39	-13.75	-13.14	-12.55
Log f_{S_2}	-10.64	- 8.04	- 6.49	- 5.26	- 4.21	- 3.28	- 2.44	- 1.65	- 0.92	- 0.23	+ 0.42
800°C											
Log f_{O_2}	-18.75	-16.85	-15.71	-14.81	-14.04	-13.33	-12.70	-12.10	-11.53	-11.00	-10.50
Log f_{S_2}	- 9.13	- 6.61	- 5.14	- 4.00	- 3.03	- 2.18	- 1.42	- 0.71	- 0.06	+ 0.54	+ 1.12
900°C											
Log f_{O_2}	-16.46	-14.61	-13.53	-12.68	-11.96	-11.32	-10.74	-10.20	- 9.69	- 9.21	- 8.75
Log f_{S_2}	- 7.89	- 5.42	- 4.02	- 2.95	- 2.05	- 1.27	- 0.57	+ 0.06	+ 0.65	+ 1.18	+ 1.69

Note: Many of the above points are metastable due to the stability of other compounds such as wustite, fayalite, pyrite, or sulfur liquid.

Pressure Correction

The effect of pressure on the pyrrhotite-magnetite boundary may best be estimated by calculating the shift of the triple point, iron-magnetite-troilite, from which the curve originates. The effects of pressure on the slope of the curve are dependent on the change in composition of the pyrrhotite for a given sulfur fugacity. This variation is not known, but would cause a change in the boundary which is an order of magnitude less than that caused by the shift in the origin and can therefore be ignored.

The sulfur fugacity of the triple point is defined by the reaction

(29) $2\ Fe + S_2 = 2\ FeS$

(30) $(\log f_{S_2})_o = -\log K = \frac{\Delta G}{2.303\ RT}$

where ΔG is defined at 1 bar pressure. To model a change in pressure, a $P\Delta V$ term may be added to the ΔG of the reaction.

(31) $(\log f_{S_2})_o^P = \frac{\Delta G}{2.303\ RT} + \frac{\Delta V_1 (P-1)}{2.303\ RT}$

where ΔV_1 is the change in volume of the solids in reaction (29). The shift in sulfur fugacity is therefore equation (31) minus (30):

(32) $\Delta(\log f_{S_2})_o^P = \frac{\Delta V_1 (P-1)}{2.303\ RT} \cong \frac{\Delta V_1 P}{2.303\ RT}$

where the last approximation is appropriate for large P (100 bars or so).

The oxygen fugacity of the triple point is also offset, which will give an apparent change in sulfur fugacity for a specific oxygen value. This shift takes the form

(33) $3/2\ Fe + O_2 = 1/2\ Fe_3O_4$

(34) $(\log f_{O_2})_o = -\log K = \frac{\Delta G}{2.303\ RT}$

(35) $\Delta(\log f_{O_2})_o^P = \frac{\Delta V_2 (P-1)}{2.303\ RT} \cong \frac{\Delta V_2 P}{2.303\ RT}$.

For our purposes, it is useful to represent both changes as a shift in log f_{S_2} at a fixed log f_{O_2}. The shift in $(\log f_{O_2})_o$ must therefore be offset by a change of log f_{S_2} along the curve, which near the starting point will be that for stoichiometric FeS:

(36) $\Delta(\log f_{S_2}) + \frac{d(\log f_{S_2})}{d(\log f_{O_2})} \cdot \Delta(\log f_{O_2})_o^P = 0$

(37) $\Delta(\log f_{S_2}) = -4/3\ \Delta(\log f_{O_2})_o^P$.

Adding the effects of equations (32) and (37) we obtain the following:

(38) $\Delta(\log f_{S_2})_{total}^P = \Delta(\log f_{S_2})_o^P - 4/3\ \Delta(\log f_{O_2})_o^P$,

(39) $\Delta(\log f_{S_2})_{total}^P = \frac{\Delta V_1 P}{2.303\ RT} - 4/3\ \frac{\Delta V_2 P}{2.303\ RT}$.

Since the compressibilities and thermal expansions are minor correction for solids at crustal pressures, they may be ignored and the volumes at 1 bar and 25 °C substituted without significant error (Barton, 1970). The values of both terms, and the resulting $\Delta(\log f_{S_2})_{total}^P$ calculated in this way are tabulated in Table A-2 as a function of temperature for a 1000 bar change in pressure. In the equations of this paper, the $\Delta(\log f_{S_2})_{total}^P$ per kilobar will be given the symbol (A).

Table A-2. Pressure effect on the pyrrhotite–magnetite boundary

T(°C)	$\frac{\Delta V_1 \times 1000}{2.303\ RT}$	$\frac{\Delta V_2 \times 1000}{2.303\ RT}$	$\Delta(\log f_{S_2})_{total}$ per kilobar (A)
600	0.133	0.070	0.040
700	0.119	0.062	0.036
800	0.108	0.057	0.032
900	0.099	0.052	0.030
1000	0.091	0.047	0.028

Note: Volume data from Robie et al. (1979).

Effect of Solid Solutions in Pyrrhotite and Magnetite

The effect of solid solution of other cations in place of iron in pyrrhotite and magnetite can also be modelled by considering the offset of the origin of the curve, namely the iron-magnetite-troilite triple point. In the case of pyrrhotite, the effects of iron deficiencies are already considered in the integration, so the dominant effect to evaluate is the substitution of iron. The effect of pyrrhotite solid solution on sulfur fugacity thus becomes:

(40) $(\log f_{S_2})_o = -\log K + 2 \log a_{FeS}$

(41) $\Delta(\log f_{S_2})_o = 2 \log a_{FeS}$.

To a good approximation, the a_{FeS} may be replaced by the mole fraction of iron in the iron site

(42) $a_{FeS} = \frac{N_{Fe}}{N_{cations}} = X_{Fe}^{po}$.

Therefore the effect of substitution for iron on sulfur fugacity is

(43) $\Delta(\log f_{S_2})_o = 2 \log X_{Fe}^{po}$,

and those for SO_2 and H_2S become

(44) $\Delta(\log f_{SO_2}) = \Delta(\log f_{H_2S}) = \log X_{Fe}^{po}$.

Solid solution in magnetite will cause a change in the oxygen fugacity of the triple point, and thus the magnetite-pyrrhotite curve. From equations (33) and (34), this relationship becomes

(45) $(\log f_{O_2})_o = -\log K + 1/2 \log a_{Fe_3O_4}$

(46) $\Delta(\log f_{O_2})_o = 1/2 \log a_{Fe_3O_4} = 1/2 \log X_{Fe_3O_4}^{mag}$

where $X_{Fe_3O_4}^{mag}$ is the mole fraction of Fe_3O_4 in magnetite as defined by an appropriate solution model, for example Stormer (1983). For our purposes, it is convenient to represent this shift in oxygen fugacity as its equivalent offset of sulfur fugacity along the magnetite-pyrrhotite boundary, as was done in the pressure correction (36 and 37).

(47) $\Delta(\log f_{S_2}) + \frac{d(\log f_{S_2})}{d(\log f_{O_2})} \cdot \Delta(\log f_{O_2}) = 0$

(48) $\Delta(\log f_{S_2}) = -4/3\ \Delta(\log f_{O_2}) = -2/3 \log X_{Fe_3O_4}^{mag}$.

The equivalent shifts in log f_{SO_2} and log f_{H_2S} are

(49) $\Delta(\log f_{SO_2}) = \Delta(\log f_{H_2S}) = -1/3 \log X_{Fe_3O_4}^{mag}$.

In an analogous manner, the change in position of the fayalite - pyrrhotite curve can be calculated for use in compositions which contain fayalite rather than magnetite. Analogous curves can also be calculated for other iron-silicate-pyrrhotite assemblages as long as all phases can be characterized thermodynamically.